Multibody modelling of ligamentous and bony stabilizers in the human elbow

Mara Terzini[1]
Elisabetta Maria Zanetti[2]
Alberto Luigi Audenino[1]
Giovanni Putame[1]
Laura Gastaldi[1]
Stefano Pastorelli[1]
Elisa Panero[1]
Arman Sard[3]
Cristina Bignardi[1]

[1] Department of Mechanical and Aerospace Engineering, Politecnico di Torino, Torino, Italy
[2] Department of Engineering, University of Perugia, Perugia, Italy
[3] Hand Surgery Division, AOU CTO, Turin, Italy

Corresponding author:
Mara Terzini
Department of Mechanical and Aerospace Engineering
"Politecnico di Torino"
Corso Duca degli Abruzzi 24
10129 Torino, Italy
E-mail: mara.terzini@polito.it

Summary

The elbow ligamentous and bony structures play essential roles in the joint stability. Nevertheless, the contribution of different structures to joint stability is not yet clear and a comprehensive experimental investigation into the ligament and osseous constraints changes in relation to joint motions would be uphill and somehow unattainable, due to the impossibility of obtaining all the possible configurations on the same specimen. Therefore, a predictive tool of the joint behavior after the loss of retentive structures would be helpful in designing reconstructive surgeries and in pre-operative planning. In this work, a multibody model consisting of bones and non-linear ligamentous structures is presented and validated through comparison with experimental data. An accurate geometrical model was equipped with non-linear ligaments bundles between optimized origin and insertion points. The joint function was simulated according to maneuvers accomplished in published experimental studies which explored the posteromedial rotatory instability (PMRI) in coronoid and posterior medial collateral ligament (PB) deficient elbows. Moreover, a complete design of experiments (DOE) was explored, investigating the influence of the elbow flexion degree, of the coronoid process and of the medial collateral ligaments (MCL) structures (anterior and posterior bundles) in the elbow joint opening. The implemented computational model accurately predicted the joint behavior with intact and deficient stabilizing structures at each flexion degree, and highlighted the statistically significant influence of the MCL structures ($P<0.05$) on the elbow stability. The predictive ability of this multibody elbow joint model let foresee that future investigations under different loading scenarios and injured or surgically reconstructed states could be effectively simulated, helping the ligaments reconstruction optimization in terms of bone tunnel localizations and grafts pre-loading.
Level of evidence: V.

KEY WORDS: elbow stability, medial collateral ligaments, coronoid process, multibody model.

Introduction

The elbow joint comprises ligamentous and bony stabilizers that furnish both primary and secondary stability during flexion. The ulnohumeral articulation, the anterior bundle of the medial collateral ligament (AMCL) and the lateral collateral ligament (LCL) complex are the 3 primary static constraints, while the radiocapitellar articulation, the common flexor tendons, the common extensor tendons and the joint capsule are the secondary static constraints[1]. The muscles which cross the elbow joint represent the dynamic stabilizers, and their role has already been investigated in[2,3]. The full flexion-extension of the elbow ranges between 0° at extension and 140° at maximum flexion, nevertheless the range required for daily activities is reduced to 20°-120°. At this flexion degrees, the elbow stability is dependent on medial collateral ligament (MCL), while interlocking of the bony anatomy furnishes constraints for lower and higher flexion degrees. The MCL complex is composed of three ligamentous structures: the Anterior Bundle (AB), the Posterior Bundle (PB) and the Transverse Bundle (or Cooper's ligament). The Transverse Bundle (TB) is commonly considered not involved in the elbow stability[4]. The tensions and stabilizing functions of liga-

ments vary according to the amount and type of motion. Generally, when no varus or valgus stress is applied, the anterior portion of the AB is taut between 0° and 50° while the posterior portion of the AB is in tension from 85° of normal flexion. A middle portion of the AB appears taut throughout a wide range of motion, and for this reason it is considered an isometric band. Conversely, the PB works from about half flexion to full flexion[5]. The undisputed importance of the AB as a primary stabilizer of the elbow to valgus stress was investigated by several Authors[6-8], and up to present days, in simple unstable or complex dislocations, the reconstruction techniques (such as the modified Jobe technique, the docking technique and the hybrid interference screw fixation technique) addresses the AB only[9]. Although the PB role in elbow stability has not been clearly defined yet, it is always injured in dislocated elbows and is sacrificed (or not reconstructed) in many common surgical procedures, both due to its position and its specific fan-shaped structure. In the last decade, the importance of the PB in elbow stability was investigated deeper, starting from a study aimed at the determination of the effect of PB sectioning in varus and posteromedial rotatory instability (PMRI)[10]. A reconstruction attempt of the PB only was proposed in the treatment of the posteromedial rotatory instability as a solution for a posteromedial olecranon deficiency in a Major League athlete[11]. Recent studies[12, 13] demonstrated the significant PB role as a secondary stabilizer of valgus instability and in preventing the posterior dislocation of the elbow.

Anyhow, any reconstruction procedure aims at the restoration of the original joint stability, and since ligaments stabilizing tensions change with the motion amount and type, a thorough knowledge of osseous interactions and ligaments function is necessary. However, an exhaustive experiment into the ligament constraints changes in relation to joint motions would be cost and time consuming, even considering a subset of the possible configurations[14]. An advantageous solution would be the use of computational modeling, that has become an important tool for the characterization of complex systems. These models allow for the quantitative evaluation of anatomical and physiological parameters in a potentially infinite number of configurations, eliminating the need for many samples and greatly reducing costs. As an example, through a model it is possible to evaluate the influence of a ligament at a time on a specific elbow, which is impossible in an experimental framework. Moreover, validated models can be used to investigate and optimize surgical procedures in a virtual setting[15]. The multibody analysis is the ideal methodology to be used for such dynamic simulations because of its computational efficiency. In fact, in this framework the contact mechanics are highly simplified and the non-linear structures can be approximated through mathematical formulations. Obviously, involving rigid body analysis, no stress computation is performed, and the systems studied with this methodology must undergo negligible deformations. Anyhow, flexible bodies involving geometrical and material non-linearities could be implemented in a multibody simulation combining the rigid-body framework with the finite element analysis.

The purpose of this study was to develop in the multibody framework an anatomically detailed elbow joint model provided with non-linear ligaments. The model performances were evaluated through comparison between the model kinematics and experimental measurements collected from literature.

Materials and methods

A multibody model was created in ADAMS (MSC Software Corporation, Santa Ana, CA) by importing the CAD geometry of a medium-size physiological human right arm, composed of humerus, ulna and radius. The bones geometries, derived from database, were pre-assembled in the extended position. A density of 1600 kg/m^3 was used for the osseous components[16].

Ligaments formulation - Regarding the medial collateral ligament complex (MCLC), the model included two bundles for the anterior part (AB) and two bundles for the posterior part (PB). The lateral collateral ligament complex (LCLC) comprises two bundles for the radial collateral ligament (RCL), two bundles for the annular ligament and one bundle for the lateral ulnar collateral ligament. The interosseous membrane (IOM) was divided into five bundles: the proximal and the distal accessory band, the proximal and the distal central band and the distal oblique cord. Finally, the distal radioulnar ligaments (DRULs) were modelled with a dorsal and a palmar bundle. Both localization and stiffness of implemented ligaments were obtained through anatomic and biomechanical data found in literature[5,17-22]. In fact, ligaments were attached to the bones through an iterative procedure aimed at optimizing the insertion point localization according to the desired ligaments activation ranges and force trends (e.g. the anterior AB has a decreasing trend in its activation range, while the posterior PB has a growing trend). For this purpose, in the first phase the ligaments have been approximated with springs, and the forces generated in normal, valgus and varus flexion were monitored and compared with the activation ranges described in Regan study[5]. The optimization procedure was completed when the activation ranges were comparable to those summarized in Table I. Ligaments and intraosseous membrane were then modeled as non-linear springs thanks to the implementation of user-defined functions (Eq. 1) describing their load (L) - strain (ε) relation.

$$= \begin{cases} 0 & \varepsilon < 0 \quad zero - strain\ region \\ -\frac{1}{4}K\frac{\varepsilon^2}{\varepsilon_L} & 0 \le \varepsilon \le 2\varepsilon_L \quad toe\ region \\ -K(\varepsilon - \varepsilon_L) & \varepsilon > 2\varepsilon_L \quad linear\ region \end{cases}$$

The relation described in Equation 1 highlights a toe region characterized by a parabolic transition from the zero-strain region to the linear region, which simulates

Table I. Ligaments bundle properties (n/a identifies isometric ligaments which are active throughout the motion).

ID	Tissue bundle	Ligaments	Range of Action [°]			Stiffness (N/mm)
			Neutral	Valgus	Varus	
A-a	MCLC [5]	Anterior AB	0-50	0-85	0-30	36.15
B-b		Posterior AB	85-140	55-140	100-140	36.15
C-cd		Anterior PB	80-140	65-140	90-140	26.00
D-cd		Posterior PB	100-140	90-140	105-140	26.00
E-e	LCLC [5]	Anterior RCL	0-40	0-48	0-52	23.25
FG-f		Posterior RCL	90-140	90-140	70-140	23.25
FG-g		Ulnar	105-140	117-140	0-140	57.00
N-n		Anterior Annular		n/a		57.00
P-p		Posterior Annular		n/a		57.00
O-o	DRULs [17]	Dorsal		n/a		13.2
H-h		Palmar		n/a		11.00
I-ij	IOMÈ	Oblique cord		n/a		65.00
M-m	[18, 19, 20]	Proximal Accessory band		n/a		18.90
L-l		Distal Accessory band		n/a		18.90
K-k		Proximal Central band		n/a		65.00
J-ij		Distal Central band		n/a		65.00

the progressive alignment of collagen fibers along the loading direction (Fig. 1). The stiffness parameters K for each bundle were defined from literature[5,17-20] and are summarized in Table I. The spring parameter ε_L was assumed to be 0.03[16,23-26]. Moreover, a parallel damper with a damping coefficient of 0.5 Ns/mm was added to the formulation: the damping effect does not alter the load-strain relation but helps to remove eventual high frequency noise during the simulation[26].

The zero-load length used in the engineering strain (ε) calculation was obtained as a point-to-point measure between the origin and the insertion point in the static extended position for isometric ligaments, while the non-isometric ones have needed several preparatory simulations in order to be able to bring the articulation to the correct flexion degree. For example, in normal flexion the anterior AB is taut in the flexion range between 0° and 50°, and consequently it will behave lax for higher degrees[5]. Thus, the initial length for the anterior AB was measured with the elbow joint positioned at 50° of flexion. The final insertion points of the modeled ligaments and intraosseous membrane are shown in Figure 2.

Articular contact - The contact force between the bodies completes the multibody model definition, and de-

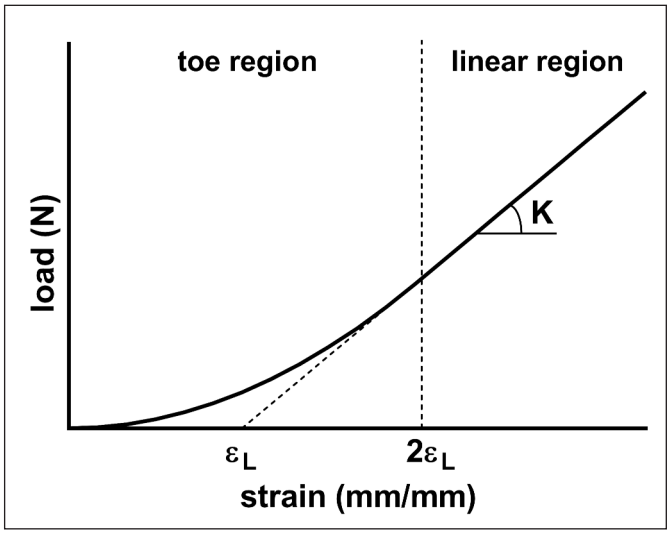

Figure 1. Typical load-strain relation for ligaments, as formulated in Equation 1: the initial toe region is characterized by a parabolic trend while, for $\varepsilon > 2\varepsilon_L$, the load is linearly related to the strain through the stiffness K.

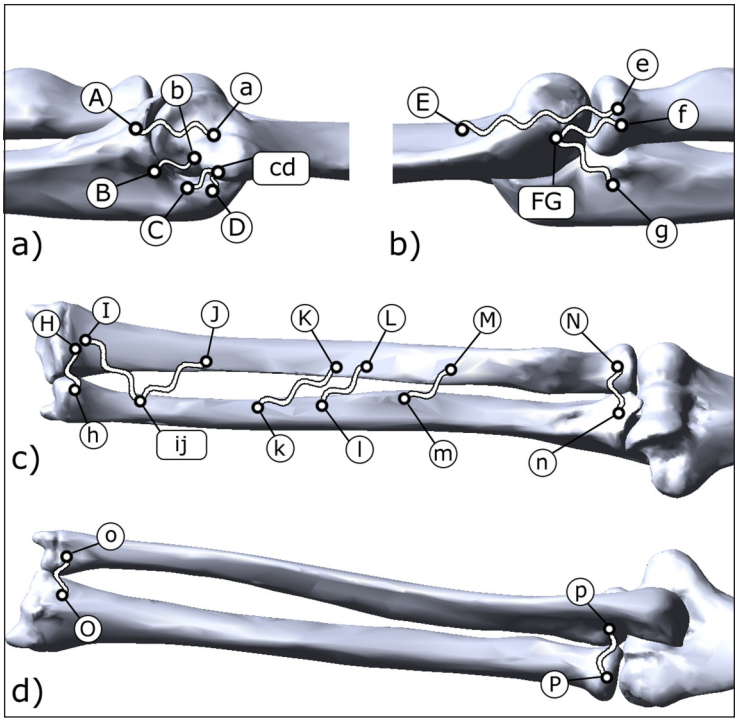

Figure 2 a-d. Ligaments origin and insertion points on humerus, radius and ulna shown in the medial view (a), lateral view (b), top view (c) and bottom view (d). Uppercase and lowercase letters identify origins and insertions of each bundle as listed in Table I.

scribes the interaction between the bones of the upper limb. In the geometrical model the articular cartilage wasn't included, and the presence of this deformable body was fictitiously reproduced through a compliant contact between the osseous components, greatly reducing computational costs. Humerus-ulna, humerus-radius and ulna-radius contact forces were therefore defined through an impact formulation (Eq. 2) describing the contact force F_c as a function of the interpenetration between bodies (δ) and the interpenetration velocity (δ) .

$$F_c = k \cdot \delta^e + c(\delta) \cdot \dot{\delta}$$

In Equation 2, *k* is the contact stiffness, *e* is the nonlinear power exponent and *c(*δ*)* is the damping coefficient. To prevent discontinuities in the solution at the initial contact, the damping coefficient is a function of the interpenetration δ. In fact, the dissipative component of the contact force contains a Heaviside step function, approximated with a cubic polynomial, which modulates the damping coefficient from zero when contact first occurs, to a maximum value, equal to *c*, when the interpenetration is equal to *d* (Fig. 3). Therefore, for greater interpenetrations the damping coefficient will maintain a constant value. The contact parameters, defined through literature[27, 28], are listed in Table II. The contribute of friction was neglected due to the low frictional coefficient caused by the synovial fluid presence[29, 30].

Maneuvers set-u - The model optimization in terms of ligaments insertion points localization needed a specific motion simulation aimed at the execution of the flexion-extension and varus-valgus maneuvers. Mimicking the clinician hand on the patient wrist, a ring was positioned in the model and its dimensions were optimized to guide the movement of the forearm without over-constraining it (Fig. 4). In particular, the varus-valgus movement was obtained through a translation of the ring along the Z axis, while the flexion movement is guided by a revolute joint positioned near the elbow joint. This artifice made it possible to provide the desired movements while retaining the physiological elbow rotation centers. The humerus body was constraint with a fixed joint to the *ground* and it was considered as a motionless reference for the whole study.

Model validation **-** The model validation consisted in reproducing the experimental measurements described in two recent investigations which tested cadaveric elbows applying an axial compression with varus and internal rotation torque[13, 31]. The experimental maneuvers performed by Gluck et al.[31] and Golan et al.[13] were reproduced at 30°, 60° and 90° of flexion, imposing an axial compression along the ulnar axis (10 N and 25 N respectively), with varus (5°) and internal rotation torque (2.5 Nm). In detail, the simulation starts with the flexion movement, provided by a revolute joint assigned to the motion ring, until the set angle is reached (Fig. 5a). Subsequently, a second translational joint rotates the forearm in the frontal plane until it reaches 5° of varus (Fig. 5b). Finally, a compression force (Fig. 5c) followed by an internal rotation torque (Fig. 5d) are applied along the

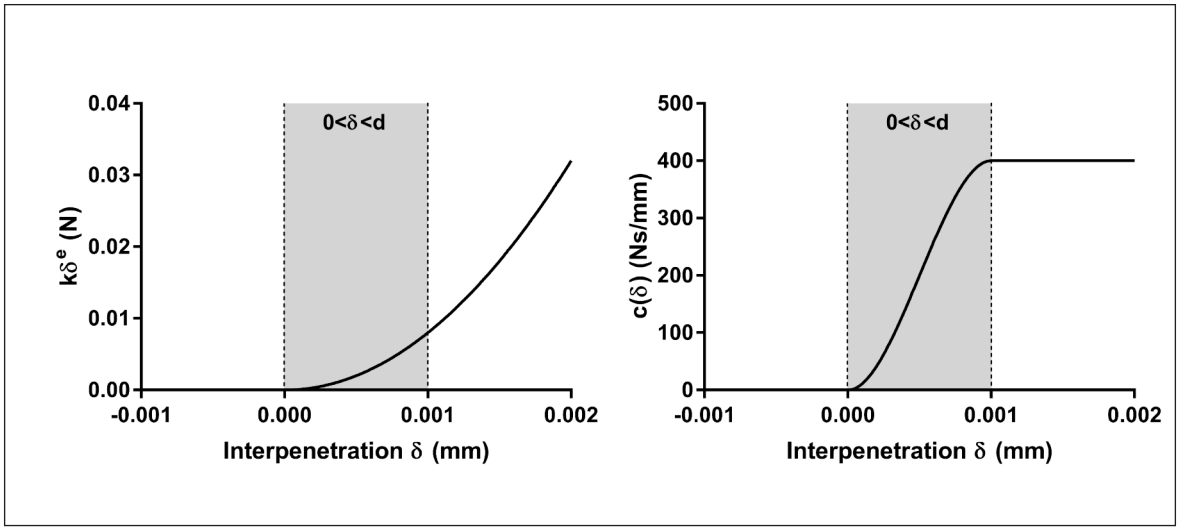

Figure 3. Elastic (left) and damping (right) contributes of the impact function (Eq. 2). The grey region is referred to the interpenetration between the bodies from the initial contact (δ=0) to the interpenetration δ=d, where the damping coefficient reaches its maximum value c.

Table II. Humerus-ulna, humerus-radius and ulna-radius contact parameters.

Parameter	Value
Contact type	Impact
Contact stiffness (*k*)	8000 N/mm
Exponent (*e*)	2
Damping Coefficient (*c*)	400 Ns/mm
Interpenetration of geometries (*d*)	0.001 mm

ulnar axis. These four loads, which sequentially generate the dislocation maneuver, have a duration of 2 seconds each (for a total of 8 seconds of simulation) and are modulated by a cubic polynomial which helps to prevent discontinuities in the solution. During the entire dislocation maneuver, the humerus is rigidly fixed to the *ground*. To recreate the experimental conditions of Gluck's work, a 50% coronoid cut has also been modelled (Fig. 6), even though the joint capsule modelling has been here avoided for simplicity. The radial osteotomy performed in the reference works to prevent hinging around the fixed radius was here avoided. In fact, the osteotomy role was to discharge the excessive constraint generated by the polymer casting used as a constraint to the testing machine, which in this multibody model is unnecessary as the ring action allows physiological movements between ulna and radius. For each of the two geometrical models (intact coronoid and coronoid cut), different ligament configurations were simulated: intact ligaments, AB cut, PB cut and MCLC cut. This latter consisted in the deactivation of the four bundles (AB+PB) of the medial collateral ligament complex. Maneuver outcomes were evaluated in the medial side of the elbow joint where a set of four markers were placed to allow the tracking of the ulno-humeral

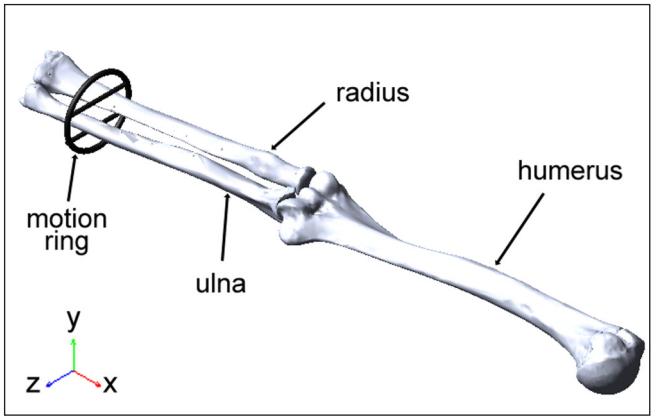

Figure 4. Complete geometrical model composed of humerus, radius and ulna pre-assembled in the extended position. Mimicking the clinician hand, the motion ring (in black) is positioned at the wrist level.

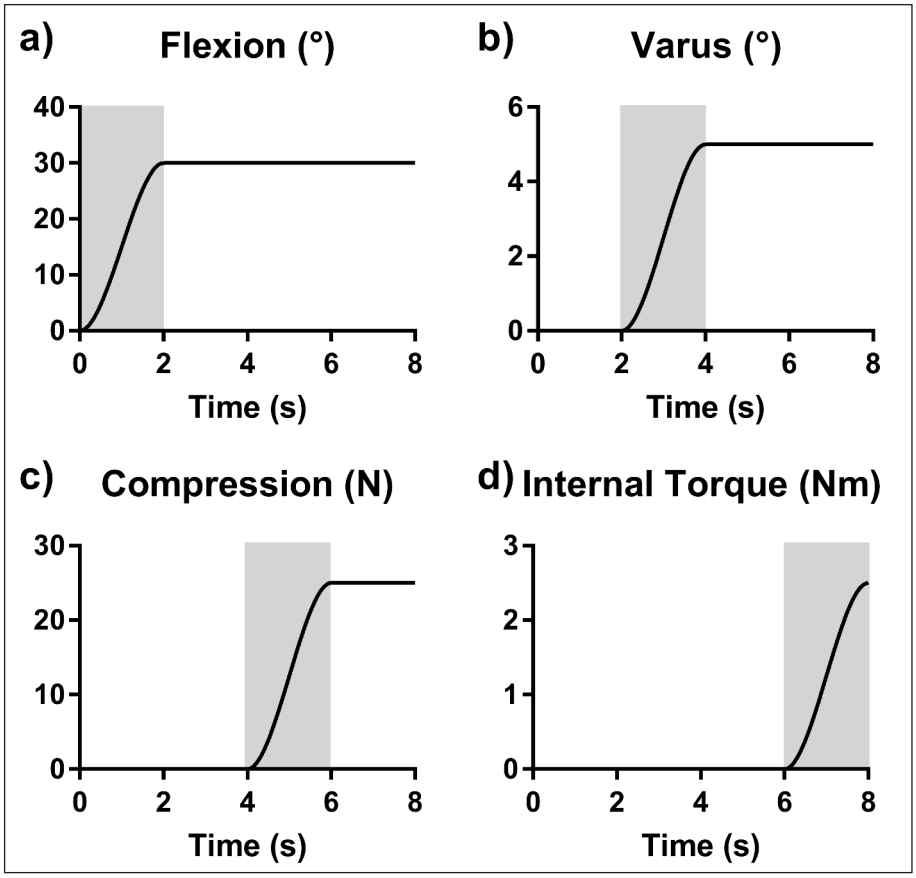

Figure 5 a-d. Loads and displacements applied to the forearm in the dislocation maneuver: a) flexion of the forearm from full extension (0°) to the set angle (30°, 60° or 90°); b) varus motion in the frontal plane from 0° to 5°; c) compression force along the ulnar axis (from 0 to 10 N or 25 N); d) internal rotation torque around the ulnar axis (from 0 to 2.5 Nm).

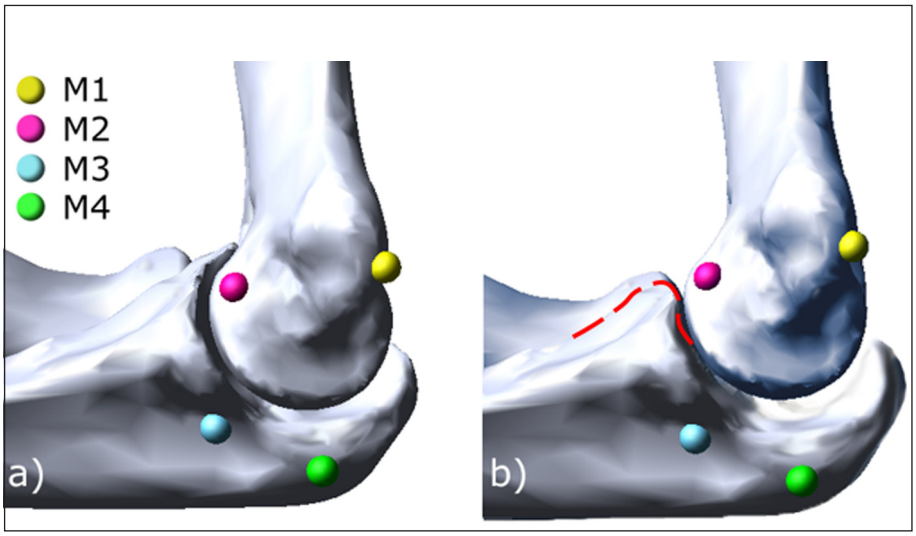

Figure 6 a,b. Markers placement in the intact model (a) and in a 50% coronoid cut model (b): the M2-M3 distance increment following the maneuver is the distal gap while the M1-M4 distance increment is the proximal gap, used in the model validation.

joint in terms of joint opening in the distal and in the proximal region (Fig. 6). Markers for the proximal gap evaluation were placed on the distal medial trochlea (M2) and on the proximal extent of the sigmoid notch (M3); markers for the distal gap evaluation were placed on the medial epicondyle (M1) and on the distal extent of the sigmoid notch (M4). Joint openings were thus measured as the distance increment at the simulation end with respect to the marker distance at the time of initial forearm flexion, since this instant defines the beginning of the actual dislocation maneuver.

Statistical analysis - A multiple regression analysis has been performed setting the flexion angle (three levels: 30, 60 and 90°), the coronoid cut, the PB cut and the AB cut (two levels: intact and cut) as independent variables; second and third degrees interactions were not included. A multivariate Analysis of Variance (ANOVA) with significance level set at a standard value ($P \leq 0.05$) was performed to investigate the statistical significance of each regression variable.

Results and discussion

Similar outcomes resulted from the two set of simulations performed with 10 N or 25 N of axial compression (average deviation of about 4%), with slightly larger joint openings obtained with the higher compression force. However, in the two configurations the statistical significance of the four analyzed factors remained substantially unchanged, therefore, only results obtained with the higher compression force will be here presented. Considering the intact coronoid model, gaps prediction compared well with experimental measurement[13] and shows an opening increment from 30° to 90° of flexion after the posterior bundle cut (Fig. 7). The coronoid excision always causes a gap increment, with a preponderant effect at lower flexion degrees. The effect of the coronoid absence alone is clearly visible in Figure 8 which shows the gap increment with respect to the intact elbow. A maximum increment of 5.21 mm was obtained proximally at 30° of flexion, as a result of the coronoid osteotomy alone, while decreasing openings resulted at higher degrees. The coronoid stabilizing role is also visible when the posterior bundle is deactivated: even though the PB retaining effect has a major evidence at higher flexion degrees (i.e. in its activation range), the concomitant absence of the posterior bundle and the coronoid generates a strong instability even at lower flexion angles. Our findings agree with Gluck's work[31], which showed a not significant contribute of the PB at 30° and a rising significant gap as the flexion increases. It should be noted that a significant interaction between the coronoid cut and the PB cut emerges, since an increasing gap caused by the PB cut in the model with a 50% coronoid osteotomy is clearly visible as the flexion increases. In fact, the high gap resulting at 30° of flexion is almost entirely generated by the coronoid absence, and the additional PB resection generates a gap increment of about 2.6% both distally and proximally with respect to the model with the coronoid cut only, while it increases up to 43% at 60° of flexion, even reaching 187% of increment for the distal gap at 90°. Conversely, Golan et al.[13] highlights a significant role of the PB in the elbow stability at 30° with the contribute of an intact coronoid. The findings of the two references are, in the Authors opinion, contradictory, even because experimental evidences demonstrated the coronoid constraining role at lower flexion angle under varus stress[32].

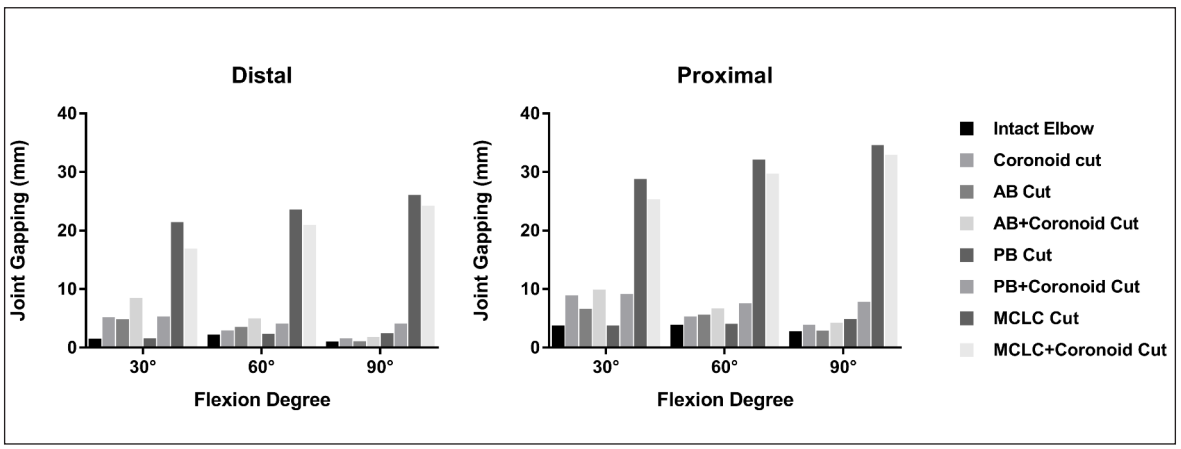

Figure 7. Distal (left) and proximal (right) joint gap at 30°, 60° and 90° of flexion. In black are represented the intact elbow with intact ligaments results (used as control) while "Coronoid Cut" is the 50% coronoid cut model with intact ligaments. "AB Cut", "PB Cut" and "MCLC Cut" represent the anterior bundle deactivation, the posterior bundle deactivation and medial collateral ligament complex deactivation (both anterior and posterior bundles) respectively.

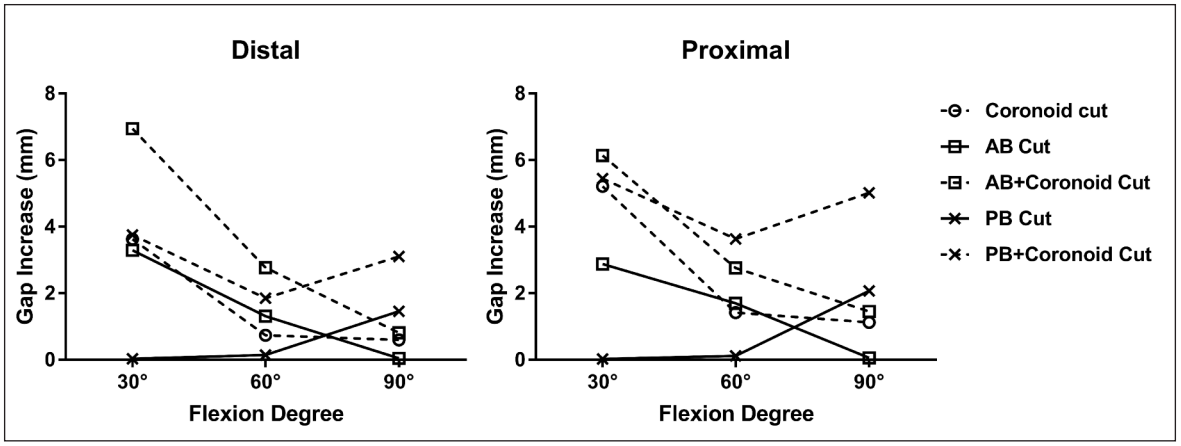

Figure 8. Distal (left) and proximal (right) gap increments with respect to the intact elbow following ligaments dissection and coronoid cut: ○ - intact ligaments; □ - Anterior Bundle dissection; × - Posterior Bundle dissection. Dashed lines are referred to the intact elbow while continuous lines are referred to the 50% coronoid cut elbow.

The multibody framework's capabilities include, among others, the possibility to explore the systems behavior under the influence of fixed factors exploring each possible configuration (DOE), and results regarding the two analyzed parameters (distal and proximal gap) for the 24 analyzed combinations (factors: flexion degree, coronoid presence, AB and PB excision) are shown in Figure 7. Considering the ligaments contribute, the deactivation of the AB causes a statistically significant increment both in the distal (P=.0002) and in the proximal (P=.0004) opening at lower degrees, while a significant (P=.0005 distally and P=.0003 proximally) contribute of the PB is visible at higher degrees. The coronoid absence has an influence at lower degrees, and its deactivation in concomitance with a ligament excision increases the openings at each flexion degrees, even though its contribute isn't statistically significant (P=.7433 distally and P=.6187 proximally). Among the investigated factors, the flexion angle doesn't play a significant role (P=.9910 distally and P=.9973 proximally), excepted when considered in its interaction with the PB factor (P=.0372). Moreover, the concomitant deactivation of the AB and the PB of the medial collateral ligament always leads to a frank elbow dislocation. Therefore, high gap values resulted from MCLC deactivation, both in the distal and in the proximal area.

The geometrical model exploited in this study was an accurate representation of a standard physiological medium size elbow joint, but several discrepancies persist between the model and the experimental configuration[13, 31]. First of all the implemented model is characterized by standard shapes and articular contact surfaces, in all likelihood different from the elbow joints tested in the *ex vivo* studies. Moreover, the geometrical model was a description of a single elbow, whereas the experimental studies involved several samples, allowing for a generalization of the results. However, the obtained results show how the standard elbow model falls within the variability of the experimental results, being an average description of the population. Secondly, the osteotomies performed by Golan and Gluck teams on the radius prejudiced the normal elbow kinematics due to the alteration not only of the radio-humeral contact force in compressive stress, but also of the action of the annular ligament and the radial collateral ligament. This latter provides a predominant support in the varus stress[33] while the annular ligament stabilizes the radio-ulnar joint and therefore doesn't directly contribute to the ulno-humeral stability. Moreover, the radial head is an important secondary varus-valgus stabilizer, and an increasing joint instability was reported in settings of radial head fracture with a MCL insufficiency[34]. Finally, the implemented model did not represent the joint capsule, which was left almost intact in the experimental reference studies. Despite the abovementioned differences, it was considered a beneficial choice the maintaining of a physiologic elbow kinematic in the present study, in order to appropriately discriminate the influence of the analyzed factors.

Regarding the ligaments modelling, load-strain relations was assumed to vary non-linearly, according to the non-linear response of collagenous tissues to loads[5]. This non-linearity was rarely included in multibody models describing the elbow kinematics, often replaced with linear formulations[27, 28]. Despite the more realistic formulation of the ligaments behavior, the stiffness values here used have been derived from the average of experimental data collected from literature[5, 17-20], and therefore they are not specific for the modeled elbow.

Anyhow, the PB role in PMRI was here confirmed, as described by several Authors[10, 13, 31], since an isolate deactivation of the posterior bundle led to an increase in joint gap at higher flexion degrees. The added coronoid resection increased the elbow instability even at lower flexion angles a confirming the PMRI occurrence in the setting of a concomitant coronoid fracture[35]. In fact, the coronoid facet lengthens the ar-

ticular surface of the elbow preventing varus instability and resisting to posteromedial rotatory forces[33]. The ulno-humeral gap in a PB-deficient joint is also in accordance with Pollock et al.[10] whose findings underline an increase in the rotatory instability after the PB excision.

The proposed model shows great promise for enlarge our understanding of the elbow biomechanics. The benefits of studying elbow kinematics by rigid body modeling are numerous. In fact, by introducing the ligament function in relation to its elongation state and the articular contact, the joint anatomical rearrangement becomes a model output, allowing for the evaluation of physiological parameters otherwise not accessible experimentally. As an example, ligament strains and contact forces acting within the articulation during daily, sporty or traumatic gestures (e.g. collisions and impacts) can be deduced. The here presented model was implemented to evaluate the ligaments and osseous components role in stabilizing the elbow joint. This virtual setting will also allow, in the light of the conclusions drawn from the study, the optimization with the CTO surgical team of a ligaments reconstruction technique which addresses both the anterior and the posterior bundles of the medial collateral ligaments, providing information about the bone tunnel localizations and the grafts pre-loading. However, with further refinement, this methodology could impact clinical biomechanics. In fact, introducing patient specific geometries[37], model outputs could be exploited in the biomechanical preoperative decision process, to guide implant design and positioning, especially in pathological elbows, characterized by peculiar articular surfaces and joint kinematic characterized by peculiar articular surfaces and joint kinematic or bone grafts from engineered bone constructs[38, 39] have been applied.

Conclusion

Aim of the study was the development and validation of an elbow model in the multibody framework capable of predicting the ligaments and osseous components role in stabilizing the elbow joint. The model validity was successfully demonstrated through comparisons of openings in the distal and in the proximal area of the elbow joint with published experimental data, even though a specific elbow geometry was investigated, without inquiring the inter-subject variability. Multibody model behavior under simulated PMRI was consistent with Golan et al. and Gluck et al. findings, even though discrepancies were found at lower flexion degrees, where the PB contribute is still debated. Anyhow, the PB role in PMRI was here confirmed since the PB cut alone led to a joint gap increase at higher flexion degrees and a strong positive interaction between the coronoid and the PB roles was highlighted. The multibody analysis has proven to be an effective and computationally efficient method for the study of the elbow joint mechanics in dynamic conditions, even in a simplified configuration. The results here presented demonstrate the model ability in predicting the ligamentous and bony stabilizers contribute in the elbow kinematics, and therefore, its potentiality in the surgical planning of joint reconstructions.

Ethics

The Authors declare that this research was conducted following basic ethical aspects and international standards as required by the journal and recently update in[40].

References

1. L Karbach, J Elfar. Elbow Instability: Anatomy, Biomechanics, Diagnostic Maneuvers, and Testing. Journal of Hand Surgery. 2017;42(2):118-126.
2. D Borzelli, S Pastorelli, L Gastaldi. Determination of the Human Arm Stiffness Efficiency with a Two Antagonist Muscles Model. Mechanisms and Machine Science. 2017;47:71-78.
3. D Borzelli, S Pastorelli, L Gastaldi. Model of the Human Arm Stiffness Exerted by Two Antagoniste Muscles. Advances in Intelligent Systems and Computing. 2017;540:285-292.
4. B Morrey, K-N An. Functional Anatomy of the Ligaments of the Elbow. Clinical Orthopaedics & Related Research. 1985;201:84-90.
5. W Regan, S Korinkek, B Morrey, K-N An. Biomechanical Study of Ligaments Around the Elbow Joint. Clinical Orthopaedics and Related Research. 1991;271:170-179.
6. R Hotchkiss, A Weiland. Valgus stability of the elbow. Journal of Orthopaedic Research. 1987;5:372-377.
7. D Eygendaal, B Olsen, S Jensen, A Seki, J Söjbjer. Kinematics of partial and total ruptures of the medial collateral ligament of the elbow. Journal of Shoulder and Elbow Surgery. 1999;8(6):612-616.
8. G Callaway, L Field, X Deng. Biomechanical evaluation of the medial collateral ligament of the elbow. The Journal of Bone and Joint Surgery. 1997;79:1223-1231.
9. G Gonzales-Lomas, N Elattrache, C Ahmad. Medial Collateral Ligament Reconstruction. In The Athlete's Elbow, Rosemont, AAOS. 2008:49-61.
10. J Pollock, J Brownhill, L Ferreira, C McDonald, J Johnson, G King. Effect of the Posterior Bundle of the Medial Collateral Ligament on Elbow Stability. Journal of Hand Surgery. 2009;34:116-123.
11. B Morrey. Reconstruction of the posterior bundle of the medial collateral ligament: a solution for posteromedial olecranon deficiency-a case report. Journal of Shoulder and Elbow Surgery. 2012;21:e16-e19.
12. D Shukla, E Golan, P Nasser, M Culbertson, M Hausman. Importance of the posterior bundle of the medial ulnar collateral ligament. Journal of Shoulder and Elbow Surgery. 2016;25;1868-1873.

13. E Golan, D Shukla, P Nasser, M Hausman. Isolated ligamentous injury can cause posteromedial elbow instability: a cadaveric study. Journal of Shoulder and Elbow Surgery. 2016;25:2019-2024.
14. Borzelli D, L Gastaldi, C Bignardi, A Audenino, M Terzini, A Sard, S Pastorelli. Method for Measuring the Displacement of Cadaveric Elbow After the Section of Medial Collateral Ligament Anterior and Posterior Bundles. Mechanisms and

Machine Science. 2018;49:972-979.
15. E Zanetti, M Terzini, L Mossa, C Bignardi, P Costa, A Audenino, A Vezzoni. A structural numerical model for the optimization of double pelvic osteotomy in the early treatment of canine hip dysplasia. Veterinary and Comparative Orthopaedics and Traumatology. 2016;30(4).
16. M Rahman, A Cil, A Stylianou. Prediction of elbow joint contact mechanics in the multibody framework. Medical Engineering and Physics. 2016;38:257-266.
17. F Schuind, K-N An, L Berglund, R Rey, WP Cooney III, RL Linscheid, EYS Chao. The distal radioulnar ligaments: A biomechanical study. The Journal of Hand Surgery. 1991;16(6):1106-1114.
18. R Hotchkiss, K-N An, D Sowa, S Basta, A Weiland. An anatomic and mechanical study of the interosseous membrane of the forearm: Pathomechanics of proximal migration of the radius. The Journal of Hand Surgery. 1989;14:256-261.
19. M Gabriel, H Pfaeffle, K Stabile, M Tomaino, K Fischer. Passive Strain Distribution in the Interosseous Ligament of the Forearm: Implications fot Injury Reconstruction. The Journal of Hand Surgery. 2004;29(2):293-298.
20. K Noda, A Goto, T Murase, K Sugamoto, H Yoshikawa, H Moritomo. Interosseous membrane of the forearm: an anatomical study of ligament attachment locations. The Journal of Hand Surgery. 2009;34(3):415-422.
21. M Hackl, M Bercher, K Wegmann, LP Müller, J Dargel. Functional anatomy of the lateral collateral ligament of the elbow. Archives of Orthopaedic and Trauma Surgery. 2016;136(7):1031-1037.
22. J de Haan, N Schep, D Eygendaal, G-J Kleinrensink, W Tuinebreijer, D den Hartog. Stability of the Elbow Joint: Relevant Anatomy and Clinical Implications of In Vitro Biomechanical Studies. The Open Orthopaedics Journal. 2011; 5:168-176.
23. G Li, J Gil, A Kanamori, S Woo. A validated three-dimensional model computational model of a human knee joint. Journal of Biomechanical Engineering. 1999;121:657-662.
24. L Blankevoort, R Huiskes. Ligament-Bone Interaction in a Three-Dimensional Model of the Knee. Journal of Biomechanical Engineering. 1991;113:263-269.
25. D Butler, M Kay, D Stouffer. Comparison of material properties in fascicle-bone units from human patellar tendon and knee ligaments. Journal of Biomechanics. 1986;19 (6):425-432.
26. T Guess. Forward dynamics simulation using a natural knee with menisci in the multibody framework. Multibody System Dynamics. 2011;28(1):37-53.
27. E Spratley, J Wayne. Computational Model of the Human Elbow and Forearm: Application to Complex Varus Instability. Annals of Biomedical Engineering. 2011;39(3): 1084-1091.
28. J Fisk, J Wayne. Development and Validation of a Computational Muscoloskeletal Model of the Elbow and Forearm. Annals of Biomedical Engineering. 2009;37(4):803-812.
29. E Radin, P Igor. A Consolidated Concept of Joint Lubrication. Journal of Bone & Joint Surgery. 1972;54(3):607-613.
30. E Radin, P Igor, D Swann, E Schottstaedt. Lubrication of synovial membrane. Annals of the Rheumatic Diseases. 1971;30(3):322-325.
31. M Gluck, C Beck, E Golan, P Nasser, D Shukla, M Hausman. pMUCL Reconstruction Recovers Elbow Stability in the Presence of Posteromedial Rotatory Instability: a cadaveric study. In ORS 2017 Annual Meeting, San Diego, 2017.
32. J Hull, J Owen, S Fern, J Wayne, N Boardman III. Role of the coronoid process in varus osteoarticular stability of the elbow. Journal of Shoulder and Elbow Surgery. 2005;14(4):441-446.
33. M Ramirez, J Stein, A Murthi. Varus Posteromedial Instability. Hand Clinics. 2015;31(4):557-563.
34. D Beingessner, C Dunning, K Gordon, J Johnson, G King. The effect of radial head fracture size on elbow kinematics and stability. Journal of Orthopaedic Research. 2005;23:210-217.
35. M Türker, A Derincek, M Çına. Coronoid fractures and elbow instability, general review and clinical presentation. European Journal of Orthopaedic Surgery & Traumatology. 2010;20(5):353-358.
36. S O'Driscoll, J Jupiter, G King. The unstable elbow. Instructional Course Lectures. 2001;50:89-102.
37. EM Zanetti, V Crupi, C Bignardi, PM Calderale. Radiograph-based femur morphing method. Medical & Biological Engineering & Computing. 2005;43(2):181-188.
38. IE De Napoli, EM Zanetti, G Fragomeni, E Giuzio, AL Audenino, G Catapano. Transport modeling of convection-enhanced hollow fiber membrane bioreactors for therapeutic applications. Journal Of Membrane Science. 2014;471:347-361.
39. D Massai, G Cerino, D Gallo, F Pennella, MA Deriu, A Rodriguez, FM Montevecchi, C Bignardi, A Audenino, U Morbiducci. Bioreactors as engineering support to treat cardiac muscle and vascular disease. Journal of Healthcare Engineering. 2013;4(3):329-370.
40. Padulo J, Oliva F, Frizziero A, Maffulli N. Muscles, Ligaments and Tendons Journal - Basic principles and recommendations in clinical and field science research: 2016 update. MLTJ. 2016;6(1):1-5.